JOURNAL OF SOLID STATE CHEMISTRY 38, 288–296 (1981)

Raman Spectra of Lanthanide Sesquioxide Single Crystals: Correlation between *A* and *B*-Type Structures

J. GOUTERON,* D. MICHEL,† A. M. LEJUS,† AND J. ZAREMBOWITCH*

**Laboratoire de Spectrométrie Vibrationnelle L.A. 161; and †Laboratoire de Chimie Appliquée de l'Etat Solide L.A. 302, Ecole Nationale Supérieure de Chimie de Paris, 11, rue P. et M. Curie 75231 Paris Cédex 05, France*

Received September 18, 1980; in revised form December 15, 1980

Structures and Raman spectra of lanthanide sesquioxide single crystals with *A*-type trigonal structure (La_2O_3, Pr_2O_3, Nd_2O_3, Sm_2O_3) and *B*-type monoclinic structure (Sm_2O_3, Eu_2O_3, Gd_2O_3) are compared. The *B* form (C_{2h}^3 or $C2/m$, $Z = 6$) derives from the *A* form (D_{3d}^3 or $P\bar{3}m1$, $Z = 1$) by a slight lattice deformation, implying a splitting of D_{3d} and C_{3v} atomic positions into less symmetrical C_{2h} and C_s sites. This close structural relationship allows one to relate the Raman active modes of the *B*-type crystals to vibrations of the *A*-type crystals and to deduce an interpretation of the complex *B*-type spectra from those of the simpler *A*-type spectra. Furthermore, it is shown that the frequency of the modes which mainly involve metal–oxygen stretching motion increases with the lanthanide atomic number in the *A* and *B* series. This evolution is interpreted in terms of increasing compactness of the structure.

Introduction

Raman spectra of the *A*-type lanthanide sesquioxides Ln_2O_3 were first studied by Denning and Ross (1972) (*1*) on microcrystalline powder samples and by Boldish *et al.* (1976) (*2*) on Nd_2O_3 single crystals. Then, our results (*3*) on La_2O_3, Pr_2O_3, and Nd_2O_3 single crystals provided a complete assignment of polarized spectra which was appreciably different from the interpretation given in the above-mentioned works. In a recent paper, Boldish and White (*4*) reported single-crystal infrared reflectance measurements for Nd_2O_3 and polarized Raman spectra for both La_2O_3 and Nd_2O_3. Their Raman data and assignment are in agreement with our previous results.

No Raman data were available concerning the second (*B*-type) modification of Ln_2O_3 oxides. Samarium, europium, and gadolinium oxides are obtained with such a monoclinic structure. This structure is a distorted arrangement of the *A* modification which results from a displacive first-order transition occurring in these oxides at high temperature (at 1900, 2050, and 2100°C for Sm_2O_3, Eu_2O_3, and Gd_2O_3, respectively (*5*)). Raman polarized spectra were first studied on Gd_2O_3 and a complete assignment was proposed (*6*). The present results concern two other compounds with *B* structure: Sm_2O_3 and Eu_2O_3.

Because of the close relationships between *A* and *B* types, it was possible to correlate the Raman data obtained for these two modifications and to deduce an interpretation of the complex spectra of *B*-type phases from that of the more symmetric *A*-type crystals. For samarium oxide, crystals with either the *B*-type (pure Sm_2O_3) or the *A*-type structure (Sm_2O_3 stabilized by a

0022-4596/81/090288-09$02.00/0

Copyright © 1981 by Academic Press, Inc.
All rights of reproduction in any form reserved.

small addition of zirconia) were studied and allowed the comparison of *A*- and *B*-type spectra for the same compound. Furthermore, our purpose was also to verify whether the observed evolution of the stretching Raman frequencies along the *A*-type series (La_2O_3, Pr_2O_3, Nd_2O_3, and Sm_2O_3 *A*-trigonal forms) could be extended to the *B*-type series (Sm_2O_3, Eu_2O_3, and Gd_2O_3 *B*-monoclinic forms).

Experimental

B-Type single crystals of Sm_2O_3, Eu_2O_3, and Gd_2O_3 were grown by the flame fusion method (Verneuil process) from high-purity fine powders (5–10 μm) of the respective oxides (grade 99.9 for Sm_2O_3 and Gd_2O_3, 99.99 for Eu_2O_3) (*7*). The powder is discontinuously injected through the flame of an improved oxhydric torch allowing the oxides to melt (melting temperature 2345°C for Sm_2O_3, 2360°C for Eu_2O_3, 2440°C for Gd_2O_3). Such-grown crystals are cylindrical Verneuil boules which can reach a length of 30 mm and a diameter of 8–10 mm. They are transparent and orange colored for Sm_2O_3, pale pink colored for Eu_2O_3, and colorless for Gd_2O_3 (*8*). They can be easily cleaved along $\{20\bar{1}\}$ planes. (The $\{20\bar{1}\}$ planes in the monoclinic B structure correspond to the basal {0001} planes in the trigonal *A* structure).

Crystals of *A*-type Sm_2O_3 were prepared by slow cooling from the melt. Melting was achieved by direct induction of RF currents (*9*). The stabilization at room temperature of the metastable *A* form was made possible by a small addition (about 5 mole%) of zirconium dioxide.

Raman spectra were obtained from a Jobin–Yvon Ramanor HG 2S spectrometer with a Spectra Physics ionized argon laser (4 W). Spectra were recorded using various exciting lines to ensure that bands were not due to fluorescence. The slit width was kept to about 2 cm^{-1}.

Structural Relationships between *A* and *B* Modifications of Lanthanide Sesquioxides

The trigonal *A*-type structure was first determined by Pauling (*10*) and has given rise to much controversy (*11–14*). Recent neutron diffraction measurements on La_2O_3 and Nd_2O_3 confirmed the space group $P\bar{3}m1(D^3_{3d})$ $Z = 1$, and accurate values for the atomic positions were determined (*15, 16*).

The two lanthanide atoms of the unit cell are located in 2*d* Wyckoff positions of $3m(C_{3v})$ symmetry (Fig. 1).

Oxygen atoms are distributed over two different sites

—1 O(I) in 1*a* ($\bar{3}m$ or D_{3d} symmetry);

—2 O(II) in 2*d* ($3m$ or C_{3v} symmetry).

The O(I) atom is octahedrally surrounded by six lanthanide atoms. The corresponding metal–oxygen bond lengths are fairly

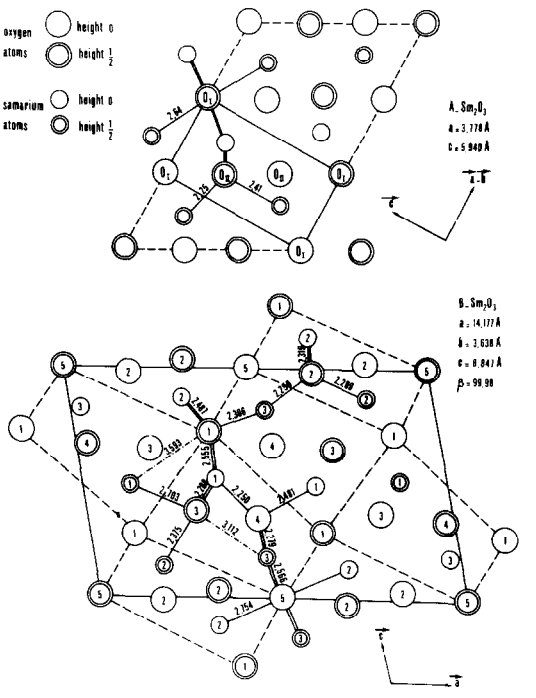

FIG. 1. Projection on the (010) plane of the monoclinic *B*-Sm_2O_3 structure and projection on the corresponding $(11\bar{2}0)$ plane of the trigonal *A*-Sm_2O_3 structure.

"long" (2.73 Å for La_2O_3 and 2,66 Å for Nd_2O_3). The O(II) atoms are surrounded by lanthanide atoms at the corners of a slightly distorted tetrahedron. Two different *Ln*–O(II) bond lengths result from the symmetry deviation $T_d \rightarrow C_{3v}$: one "short" length corresponding to three bonds (2.36 Å for La_2O_3, 2.30 Å for Nd_2O_3) and one "intermediate" length corresponding to the *Ln*–O(II) bond directed along the ternary axis (2.46 Å for La_2O_3, 2.40 Å for Nd_2O_3).

This structure may also be described as consisting of alternate slabs (perpendicular to the *c* axis) of *MO* or MO_2 composition (*M* = metal). Between two metal planes, one oxygen plane is present in the *MO* slab (oxygen atoms are located in octahedral sites as anions in NaCl structures) and there are two oxygen planes in the MO_2 slab (oxygen atoms are in tetrahedral sites as anions in CaF_2 structures). The "ideal" structure resulting from a regular intergrowth along the [111] axis of NaCl and CaF_2 slabs is reported in Fig. 2 facing the actual structure of a *A*-type compound namely Nd_2O_3.

It is interesting to notice that the experimental *c*/*a* value for *A*-type oxides increases from 1.557 for La_2O_3 to 1.572 for Sm_2O_3 and tends towards the ideal value 1.6330 ($2\sqrt{6}/3$) corresponding to a hexagonal close packing of cations (oxygen atoms O(II) in regular tetrahedral sites and oxygen atoms O(I) in regular octahedral sites).

In the *B*-type monoclinic structure, with space group $C\ 2/m(C_{2h}^3)$ the side-centered cell contains 6 Ln_2O_3 formula units (Fig. 1). Atomic positions were determined from X-ray measurements for samarium (*17*) and europium (*18*) oxides.

The 18 oxygen atoms of the unit cell occupy five different crystallographic sites:
—four in 4*i* (*m* or C_s symmetry) = O(1), O(2), O(3), O(4);
—one in 2*b* (2/*m* or C_{2h} symmetry) = O(5).
Lanthanide atoms are located in three different 4*i* positions.

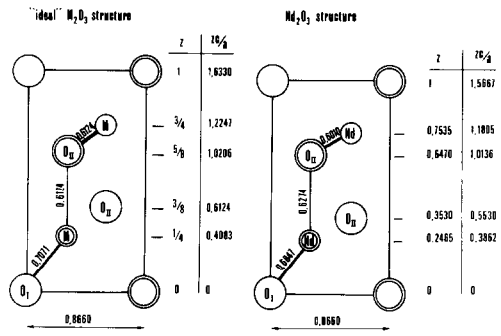

FIG. 2. Comparison between the trigonal *A*-Nd_2O_3 structure and an ideal structure with an hexagonal close-packed cationic sublattice and anions in regular sites. Projection on a $\{11\bar{2}0\}$ plane. Distances are expressed in fraction of *a*, the separation between two cations.

As shown in Fig. 1, the monoclinic cell may be considered as consisting of six distorted trigonal units (or three units for the primitive cell). Within a slight lattice deformation (a shortening of atomic separations along the [010] monoclinic axis) the *B*-monoclinic cell is related to the *A*-hexagonal cell as follows:

$$a_m = a_h - b_h + 2c_h;$$
$$b_m = -a_h - b_h;$$
$$c_m = a_h - b_h - c_h$$

(a_m, b_m, c_m are the monoclinic parameters; a_h, b_h, c_h the hexagonal parameters).

The correspondence between atomic positions in the two structures is given in Table I. Instead of an unique tetrahedral environment for O(II) oxygen atoms in the trigonal phase, three different tetrahedra more or less distorted are present in the monoclinic phase around O(2), O(3), and O(4) atoms. The site symmetry is lowered from C_{3v} to C_s. The O(I) atom positions are split into two different groups: 4 O(1) in C_s and 2 O(5) in C_{2h} symmetries.

Table II lists metal–oxygen distances around each type of oxygen atoms for monoclinic *B*-Sm_2O_3, in regard with the corresponding bond lengths in the trigonal *A*-Sm_2O_3 phase (*19*). From these data, it

TABLE I

CORRESPONDENCE BETWEEN ATOMIC POSITIONS IN THE TWO STRUCTURES

Trigonal structure		Monoclinic structure		
6 × 1 O(I)	$1a(\bar{3}m, D_{3d})$	2 O(5)	2*b*	$(2/m, C_{2h})$
		4 O(1)	4*i*	(m, C_s)
6 × 2 O(II)	$2d(3m, C_{3v})$	4 O(2)	4*i*	(m, C_s)
		4 O(3)	4*i*	(m, C_s)
		4 O(4)	4*i*	(m, C_s)
6 × 2 *Ln*	$2d(3m, C_{3v})$	4 *Ln*(1)	4*i*	(m, C_s)
		4 *Ln*(2)	4*i*	(m, C_s)
		4 *Ln*(3)	4*i*	(m, C_s)

comes out that in the monoclinic phase the environment of O(2), O(4) and O(5) atoms is very similar to that of O(II) and O(I) atoms of the trigonal phase, respectively. The main differences between the two structures are observed around O(1) and O(3) atoms:

—in the monoclinic phase O(1) atoms are only five-coordinated (lanthanide atoms at the corners of a square pyramid), whereas in the *A*-type structure the O(I) atoms have a sixfold environment.

—the O(3) atoms remain tetrahedrally coordinated and linked to 2 *Ln*(1) and 1 *Ln*(2) atoms but the fourth neighbor is a *Ln*(1) atom (in a next pseudotrigonal cell) instead of the *Ln*(3) atom of the same pseudotrigonal cell (Fig. 1).

As in the case of *A*-type structure, the evolution of the unit cell parameters shows a progressive tendency towards a more close-packed structure from Sm_2O_3 to Gd_2O_3. Because of the correspondence between *A*- and *B*-type lattices it is possible to calculate a pseudo c_h/a_h ratio for monoclinic oxides (the length $[10\bar{1}]_m$ represents 3_{C_h} and the volume of the monoclinic cell corresponds to $6a_h^2c_h3^{1/2}/2$. The values of c_h/a_h calculated from the unit cell parameters of our crystals are reported in Table III.

Correlation between Vibrational Spectra of Ln_2O_3 *A*- and *B*-Type Oxides

For trigonal oxides, four vibrational modes are active in Raman scattering ($2A_{1g} + 2E_g$) and correspond to two stretching vibrations ($A_{1g} + E_g$) and two bending modes ($A_{1g} + E_g$) of the *Ln*–O(II) bonds (3).

TABLE II

METAL–OXYGEN DISTANCES (Å) IN B-TYPE AND A-TYPE Sm_2O_3, AND MODE SYMMETRY ASSOCIATED TO EACH Sm–O STRETCHING VIBRATION

Monoclinic structure		Trigonal structure	
$O(2)Sm(2)_3Sm(3)$	1 O(2)–Sm(2) = 2,289A_g 1 O(2)–Sm(3) = 2,259A_g 2 O(2)–Sm(2) = 2,319B_g	A_{1g} 1 O(II)–Sm = 2.41 E_g 3 O(II)–Sm = 2.25	$O(II)Sm_4$
$O(3)Sm(1)Sm(2)Sm(1)_2$	1 O(3)–Sm(1) = 2,703A_g 1 O(3)–Sm(2) = 2,375A_g 2 O(3)–Sm(1) = 2,288B_g	A_{1g} 1 O(II)–Sm = 2.41 E_g 3 O(II)–Sm = 2.25	$O(II)Sm_4$
$O(4)Sm(1)_2Sm(3)_2$	1 O(4)–Sm(1) = 2,250A_g 1 O(4)–Sm(1) = 2,481A_g 2 O(4)–Sm(3) = 2,279B_g	A_{1g} 1 O(II)–Sm = 2.41 E_g 3 O(II)–Sm = 2.25	$O(II)Sm_4$
$O(1)Sm(1)_2Sm(2)_2Sm(3)$	1 O(1)–Sm(3) = 2,306 2 O(1)–Sm(1) = 2,555 2 O(1)–Sm(2) = 2,487	6 O(I)–Sm = 2.64	$O(I)Sm_6$
$O(5)Sm(2)_2Sm(3)_4$	2 O(5)–Sm(2) = 2,754 4 O(5)–Sm(3) = 2,565	6 O(I)–Sm = 2.64	$O(I)Sm_6$

TABLE III

STRUCTURAL AND SPECTROSCOPIC DATA FOR Ln_2O_3 CRYSTALS[a]

	Oxides	a (Å)	c (Å)	c/a	$\bar{\nu}$ Ln–O(II) (cm^{-1})	Average Ln–O(II) distance (Å)	Bond strength, "s"	Average O(II)–O distance (Å)
A	La_2O_3	3.936	6.128	1.557	400–408	2.39	0.57	3.02
	Pr_2O_3	3.860	6.018	1.559	406–413			
	Nd_2O_3	3.831	6.000	1.566	428–436	2.33	0.58	2.95
	Sm_2O_3	3.778	5.940	1.572	444–455	2.30	0.59	2.92

		a (Å)	b (Å)	c (Å)	β	Pseudo c_h/a_h	$\bar{\nu}$ LnO(n) n = 2,3,4(cm^{-1})	Average Ln–O(n) distance (Å)		Bond strength, "s"	Average O(n)–O distance (Å)
B	Sm_2O_3	14.18	3.624	8.855	100°0	1.582	375–572	O(2)	2.30	0.59	2.98
								O(3)	2.41	0.42	3.05
								O(4)	2.32	0.55	3.01
	Eu_2O_3	14.12	3.597	8.819	100°1	1.582	374–579	O(2)	2.28	0.60	2.96
								O(3)	2.39	0.43	3.06
								O(4)	2.30	0.55	3.00
	Gd_2O_3	14.08	3.567	8.743	100°1	1.588	385–593				

[a] Unit cell parameters (Å); extreme values of Raman frequencies (cm^{-1}) involving Ln–O(II) or Ln–O(n) stretching n = 2,3,4; mean atomic distances from (*15*) (*17–19*) around oxygen atoms in tetrahedral coordination; strength "s" of Ln–O(II) and Ln–O(n) bonds (*20*).

The distorted environment of the O(II) atoms (in C_{3v}) accounts for the splitting (A_{1g} + E_g) of the T_2 modes associated with regular tetrahedral units. A_{1g} modes are related to vibrations along the ternary axis, while E_g modes correspond to vibrations along the direction of the short Ln–O(II) bonds.

The factor group analysis for B-type crystals predicts 21 Raman active modes: $14A_g + 7B_g$.

The correlation tables between D_{3d} and C_{2h} point groups give:

$$D_{3d} \quad C_{2h}$$
$$A_{1g} \rightarrow A_g$$
$$E_g \rightarrow A_g + B_g$$

Because of the previously exposed relationships between A and B structures, three A_g modes of the monoclinic phase would be derived from each A_{1g} mode of the trigonal phase. In the same way, $3A_g + 3B_g$ modes are generated from each E_g mode. For the monoclinic phase, the A_g stretching modes correspond to atomic vibrations in the (0 1 0) plane and B_g stretching modes to out-of-plane vibrations. Thus the mode symmetry associated with the stretching vibrations of Ln–O bonds can be defined and is reported in Table II.

In addition to these modes which come from the splitting of Raman active vibrations of trigonal A-type compounds, three other modes ($2A_g + B_g$) are expected from group theory analysis. In the trigonal struc-

ture, the O(I) atoms do not participate in Raman active but only in infrared active vibrations, because they are located in centrosymmetrical positions. But this kind of oxygen atoms gives rise in the monoclinic form to O(5) atoms (also in centrosymmetrical positions) and to O(1) atoms in C_s sites. Consequently, the Raman active modes involving these O(1) atoms are expected for B-type compounds. They are derived from A_{2u} and E_u infrared active modes of A-type compounds according to the following correlation:

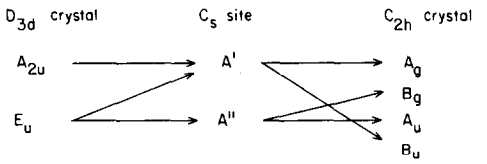

Summarizing, the 21 Raman active modes of B-type structure are derived from vibrational modes of A-type crystals according to:

$$2A_{1g} \rightarrow 2 \times 3A_g,$$
$$2E_g \rightarrow 2 \times (3A_g + 3B_g),$$
$$1A_{2u} \rightarrow 1A_g,$$
$$1E_u \rightarrow 1A_g + 1B_g.$$

Results and Discussion

A-Type Structure

The spectrum of Sm_2O_3 with trigonal structure shown in Fig. 3 is very similar to that of other A-type compounds La_2O_3, Pr_2O_3, and Nd_2O_3 (*3*). It is worth noticing the separation of A_{1g} and E_g bands at about 450 cm^{-1}. In the other Ln_2O_3 oxides, the A_{1g} line (weak and close to the E_g line) was only evidenced by polarization studies.

Our previous conclusions concerning the Raman spectra of A-Ln_2O_3 crystals are confirmed by the study of this new compound:

—at low frequency, the wavenumbers of

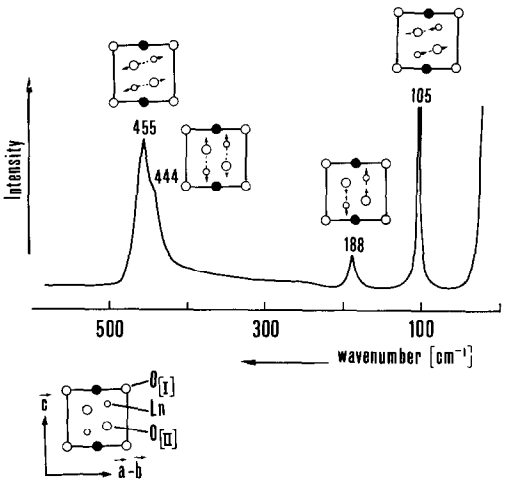

FIG. 3. Raman spectrum of unoriented A-Sm_2O_3 single crystal, λ_e = 514.5 nm, and simplified description of the modes.

the two Raman lines A_{1g} and E_g are nearly constant for the four lanthanide compounds: ~105 and ~190 cm^{-1},

—the frequencies of the stretching vibrations A_{1g} and E_g increase in the lanthanide series from La to Sm. The correlation observed between the band frequency and the c/a ratio of unit cell parameters is still obeyed for A-Sm_2O_3 as shown in Fig. 4. For these high-frequency modes, such a frequency evolution may be interpreted

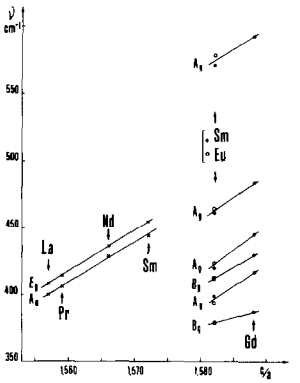

FIG. 4. Correlation between the stretching mode frequencies and the c/a and pseudo c/a ratio for lanthanide oxides with A-type (×) and B-type (○) structures, respectively.

from the variation of the a and c parameters and of characteristic interatomic distances.

The environment of the O(II) atoms, defined by the structural data for La_2O_3, Nd_2O_3, and Sm_2O_3 (*15, 19*), is characterized by the fact that the strength "*s*" of metal–oxygen bonds, calculated from bond length–bond strength empirical relations (*20*), has similar values for the different A-type sesquioxides, and that the O(II)–O distances decrease appreciably from La_2O_3 to Sm_2O_3. Average values of M–O(II) bond lengths, "*s*" bond strengths, and O(II)–O distances are listed in Table III.

Such an environment, restricted to the first and second neighbors (four cations at the corners of a tetrahedron and six anions at the corners of an octahedron respectively), is similar to the anion environment in fluorite structures with a distortion $O_h \rightarrow C_{3v}$. The frequency of the vibrational modes T_{1u} and T_{2g} of fluorite crystals was expressed by Shimanouchi (*21*). The T_{2g} Raman active mode frequency depends on two terms: a stretching constant of metal–anion bond and an anion–anion repulsion force constant. Consequently, in the case of A-type Ln_2O_3 crystals, the contribution of oxygen–oxygen repulsion appears to be sufficient to explain the increasing wavenumbers from La_2O_3 to Sm_2O_3 for modes involving O(II) atoms.

TABLE IV

RAMAN FREQUENCIES[a] AND ASSIGNMENT FOR TRIGONAL A-TYPE AND MONOCLINIC B-TYPE LANTHANIDE OXIDES

Trigonal series					Monoclinic series			
La_2O_3	Pr_2O_3	Nd_2O_3	Sm_2O_3	Symmetry	Symmetry	Sm_2O_3	Eu_2O_3	Gd_2O_3
					B_g	73	73	71
					A_g	82	84	83
					B_g	97	98	98
106	104	106	105	E_g	A_g	109	110	110
					B_g	115sh[b]	116sh	116
					A_g			123
					A_g	152	152	156
191	187	191	188	A_{1g}	A_g	175	176	175
					A_g	219	218	217
					A_g	245	246	256
		228[c]		$A_{2u} + E_u$	A_g	256	259	268
					B_g	284	285	298
					B_g	375sh	374sh	385
					A_g	378	377	387
					B_g	398	394	417
~400	~406	428	444	A_{1g}	B_g	412	413	430
408	413	436	455	E_g	A_g	420	424	445
					A_g	461	465	484
					A_g	~557sh	~575sh	583
					A_g	572	579	593

[a] in $cm^{-1} \pm 1\ cm^{-1}$.
[b] sh = shoulder.
[c] Infrared data (*4*).

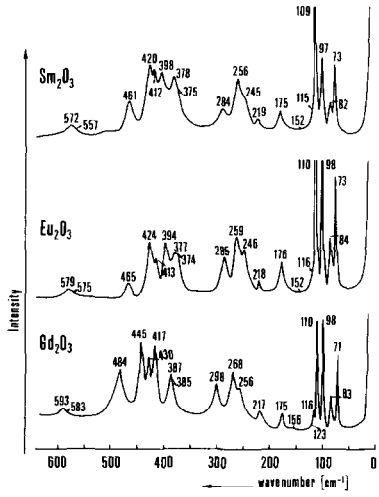

FIG. 5. Raman spectra of unoriented B-type single crystals, λ_e = 514.5 nm.

B-Type Structure

Spectra of monoclinic Sm_2O_3, Eu_2O_3, and Gd_2O_3 are reported in Fig. 5. Polarization studies performed on Gd_2O_3 crystals at low temperature, allowed the characterization of the A_g and B_g bands without any ambiguity (6). The close similarity of spectra for the three oxides leads to the assignment reported in Table IV.

B-Type spectra may be divided into four regions:

—between 70 and 125 cm^{-1}, a group of $3B_g$ and at least $2A_g$ bands (three for Gd_2O_3) is observed. In this frequency range $3B_g$ and $3A_g$ lines corresponding to $1E_g$ line located at $\sim$ 105 cm^{-1} in A-type spectra were expected.

—between 150 and 220 cm^{-1}, $3A_g$ bands are obtained corresponding to the A_{1g} line at $\sim$ 190 cm^{-1} in A-type spectra.

—between 240 and 300 cm^{-1} an isolated group of three lines ($2A_g + 1B_g$) is observed to which no Raman line corresponds in A-type spectra. These bands are assigned to the ($2A_g + B_g$) modes deriving from ($A_{2u} + E_u$) infrared active modes and involving Ln–O(1) bonds. Boldish and White (*4*) located at 228 cm^{-1} the $A_{2u} + E_u$ unsplit band in the infrared spectrum of Nd_2O_3 crystal.

—between 370 and 600 cm^{-1}, the last group of Raman lines would correspond to the splitting of the $A_{1g} + E_g$ stretching vibrations the frequencies of which are very close in the trigonal phase. Three B_g and at least five A_g lines are obtained, in good agreement with the $6A_g + 3B_g$ prediction.

The nine bands of the first two mentioned groups show a nearly constant frequency for the three oxides just as the two bands of A-type spectra from which they derive.

The modes involving Ln–O(1) bonds show a regular frequency shift (Fig. 4). Their frequencies are higher than those of the corresponding modes (infrared active) of the A-type compounds: 245 to 298 cm^{-1} as compared to 228 cm^{-1}. This can be accounted for by the fivefold coordination of the O(1) atom which supposes stronger metal–oxygen bonds. Effectively for Sm_2O_3, Sm–O(1) bond lengths are 2.555, 2.487, and 2.306 Å for the monoclinic form and 2.64 Å for the corresponding Sm–O(I) bond length in the trigonal modification.

Finally, the eight bands of higher frequency show a regular frequency shift from Sm_2O_3 to Gd_2O_3 as previously observed for the two related bands in A-type spectra. The interpretation proposed for A-type Ln_2O_3 compounds may be extended to the related B-type phases considering the evolution of the structural parameters reported in Table III. Figure 4 illustrates the splitting of the A_{1g} and E_g bands of the hexagonal form into A_g and B_g bands of the monoclinic form.

The complete description of all these vibrations would require normal coordinate analysis. This work is now in progress; however, some conclusions can already be drawn from the frequency values. For instance, the out-of-plane Sm–O bonds associated to B_g stretching modes are all longer in the B-type phase than in the A-type phase (2.319, 2.288, and 2.279 Å as com-

pared to 2.25 Å). Thus frequencies lower than 455 cm^{-1} (the trigonal E_g mode value) are expected for B_g modes of B-Sm_2O_3; effectively B_g bands appear at 375, 398, and 412 cm^{-1}. On the contrary, the shortest Sm–O distances are found in the B-form and are associated with in-plane A_g vibrations; that is consistent with the A_g symmetry determined for the two Raman lines of highest wavenumbers in the B-Sm_2O_3 spectrum.

References

1. J. H. Denning and S. D. Ross, *J. Phys. C* **5**, 1123 (1972).
2. S. I. Boldish, B. E. Scheetz, L. E. Drafall, and W. B. White, *in* "Proceedings, XII Rare-Earth Research Conference, Vail, Colorado," Vol. 2, p. 720 (1976).
3. J. Zarembowitch, J. Gouteron, and A. M. Lejus, *Phys. Status Solidi B* **94**, 249 (1979).
4. S. I. Boldish and W. B. White, *Spectrochim. Acta A* **35**, 1235 (1979).
5. M. Foëx and J. P. Traverse, *Rev. Int. Hautes Temp. Refract.* **3**, 429 (1966).
6. J. Zarembowitch, J. Gouteron, and A. M. Lejus, *J. Raman Spectrosc.* **9**, 263 (1980).
7. A. M. Lejus and J. P. Connan, *Rev. Int. Hautes Temp. Refract.* **11**, 215 (1974). A. M. Lejus, J. Cl. Bernier, and R. Collongues, *Rev. Int. Hautes Temp. Refract.* **13**, 25 (1976).
8. A. M. Lejus and R. Collongues, Lanthanide oxides, *in* "Current Topics in Materials Science" (E. Kaldis, Ed.), Vol. IV, p. 481, North-Holland, Amsterdam (1980).
9. D. Michel, M. Perez y Jorba, and R. Collongues, *J. Cryst. Growth* **43**, 546 (1978).
10. L. Pauling, *Z. Kristallogr. A* **69**, 415 (1928).
11. W. Zachariasen, *Z. Kristallogr.* **67**, 134 (1926).
12. W. C. Koehler and E. O. Wollan, *Acta Crystallogr.* **6**, 741 (1953).
13. R. W. G. Wyckoff, "Crystal Structures," Vol. II, Interscience, New York (1964).
14. H. Müller-Buschbaum and H. B. von Schnering, *Z. Anorg. Allg. Chem.* **340**, 232 (1965).
15. P. Aldebert and J. P. Traverse, *Mater. Res. Bull.* **14**, (3), 303 (1979).
16. J. X. Boucherle and J. Schweizer, *Acta Crystallogr. Sect. B* **31**, 2745 (1975).
17. D. T. Cromer, *J. Phys. Chem.* **61**, 753 (1957).
18. H. L. Yakel, *Acta Crystallogr. Sect. B* **35**, 564 (1979).
19. D. Michel and A. Kahn, to be published.
20. W. H. Zachariasen, *J. Less-Common Met.* **62**, 1 (1978).
21. T. Shimanouchi, M. Tsuboi, and T. Miyazawa, *J. Chem. Phys.* **35**, 1597 (1961); V. G. Keramidas and W. B. White, *J. Chem. Phys.* **59**, 1561 (1973).